Journal of
Polymer & Composites

ISSN: 2321-2810 (Online)
ISSN: 2321-8525 (Print)
Volume 14, Special Issue 2, 2026
DOI (Journal): 10.37591/JoPC

https://journals.stmjournals.com/jopc

Research JoPC

AI-Designed Functionally Graded Polymer Composites for Multifunctional Thin Films

D. Sai Ganesh[1,*], S.N. Padhi[2], Mamata Choudhury[3], K. Vikas[4], K. Anudeep[5]

Abstract

The design of multifunctional polymer composite thin films requires simultaneous optimization of mechanical, optical, barrier, and thermal properties—objectives often in conflict when using conventional homogeneous materials. This study presents an artificial intelligence-driven framework for designing functionally graded material (FGM) architectures in polymer nanocomposite thin films. We integrated machine learning with physics-based modeling to optimize compositional gradients across film thickness, achieving superior performance compared to homogeneous and discrete multilayer alternatives. A neural network trained on 150,000 finite element simulations and experimental data predicted material properties with R^2>0.94 accuracy. Bayesian optimization identified optimal gradient profiles for poly(methyl methacrylate) (PMMA) matrices reinforced with titanium dioxide (TiO_2) nanoparticles and functional additives. Experimental validation via layer-by-layer spin coating demonstrated 82% improvement in tensile strength, 92% optical transmittance, 47% reduction in water vapor transmission rate, and enhanced thermal stability compared to homogeneous films. The optimized FGM architecture exhibited gradual composition transitions (40-80 wt% polymer, 15-45 wt% nanoparticles across 100 μm thickness), eliminating interfacial delamination while maintaining processing feasibility. Economic analysis reveals cost-competitiveness ($28/m²) with conventional multilayer films ($22/m²) while delivering 22% higher performance index. This AI-guided approach enables rapid exploration of vast design spaces, reducing development cycles from years to weeks, and establishes a generalizable methodology for multifunctional coating applications in optoelectronics, packaging, and protective systems.

Keywords: Functionally graded materials, polymer nanocomposites, machine learning, thin films, multi-objective optimization, layer-by-layer assembly

*Author for Correspondence
D. Sai Ganesh

[1]M. Tech Student, Department of Mechanical Engineering, Koneru Lakshmaiah Education Foundation, Vaddeswaram, Guntur District, Andhra Pradesh, India
[2]Professor, Department of Mechanical Engineering, Koneru Lakshmaiah Education Foundation, Vaddeswaram, Andhra Pradesh, India
[3]Professor, Department of Computer Application, PSCMR college of Engineering and Technology, Vijayawada, Krishna District, Andhra Pradesh, India
[4,5]M. Tech Student, Department of Mechanical Engineering, Koneru Lakshmaiah Education Foundation, Vaddeswaram, Guntur District, Andhra Pradesh, India

Received Date: January 09, 2026
Accepted Date: January 20, 2026
Published Date: April 17, 2026

Citation: D. Sai Ganesh, S.N. Padhi, Mamata Choudhury, K. Vikas, K. Anudeep. AI-Designed Functionally Graded Polymer Composites for Multifunctional Thin Films. Journal of Polymer & Composites. 2026; 14(Special Issue 2): S1026–S1041p.

INTRODUCTION

Motivation and Background

Polymer composite thin films serve critical roles in modern technologies, from flexible electronics and photovoltaic encapsulation to food packaging and protective coatings. These applications demand simultaneous optimization of multiple, often competing properties: mechanical robustness for handling durability, optical transparency for display applications, barrier performance against moisture and oxygen, thermal stability for processing and service conditions, and adhesion strength for interfacial integrity [1]. Traditional approaches rely on homogeneous compositions that represent compromises across these objectives, or discrete multilayer stacks that introduce sharp interfacial discontinuities prone to delamination and optical interference.

Functionally graded materials (FGMs) offer a paradigm shift by enabling continuous, spatially varying compositions that can be tailored to achieve property gradients optimized for specific performance metrics [2]. Originally developed for thermal barrier coatings in aerospace applications, FGMs have recently gained attention in polymer systems for flexible electronics, biomedical devices, and smart coatings. However, the design space for FGM polymer composites is vast—composition profiles, particle size distributions, layer thicknesses, and processing parameters create combinatorial complexity that defies intuitive design or exhaustive experimental screening.

AI and Machine Learning in Materials Design

Artificial intelligence and machine learning have emerged as transformative tools for accelerating materials discovery and optimization. Physics-informed neural networks can learn complex structure-property relationships from limited experimental data, while evolutionary algorithms and Bayesian optimization enable efficient exploration of high-dimensional design spaces [3, 4]. Recent applications include inverse design of organic semiconductors, high-throughput screening of battery materials, and topology optimization of metamaterials. The integration of AI with traditional materials science workflows promises to reduce development times by orders of magnitude while discovering non-intuitive solutions that human designers might overlook.

In the context of polymer composites, machine learning has been applied to predict mechanical properties, optimize processing conditions, and design fiber architectures [5, 6]. However, the application of AI to functionally graded polymer nanocomposite thin films remains largely unexplored. The continuous composition gradients, thickness-dependent properties, and multi-physics coupling present unique challenges that require specialized modeling approaches and experimental validation strategies.

Natural Fiber and Hybrid Composites

Recent advances in polymer composites have explored the use of natural fibers and hybrid reinforcement systems to enhance mechanical properties while maintaining sustainability. Studies on jute fiber/polyester composites with dual fillers (eggshell powder and nanoclay) have demonstrated significant improvements in tensile, flexural, and impact strength through multi-objective optimization techniques [21]. Similarly, investigations into pineapple leaf fibers have shown their potential for automotive and structural applications, offering comparable performance to synthetic fibers while reducing environmental impact [22].

The drilling and machining characteristics of natural-fiber-reinforced composites have been extensively studied, revealing the influence of fiber orientation, stacking sequence, and processing parameters on mechanical integrity and post-drilling residual properties [23]. Furthermore, the utilization of waste materials such as manhole cover flour and medium-density fibreboard sawdust as reinforcing fillers in recycled polypropylene composites has demonstrated the feasibility of sustainable composite production with enhanced strength and water resistance [24].

Hybrid polymer composites incorporating palmyra palm leaflet and coconut sheath leaf fibers with tamarind shell powder as filler have exhibited superior mechanical performance, including enhanced tensile strength, flexural strength, and impact resistance [25]. Additionally, the treatment of natural fibers such as Acacia caesia bark with varying alkali concentrations has been shown to significantly improve tensile properties and fiber-matrix adhesion, as evidenced by fracture morphology analysis [26].

Research Objectives and Contributions

This study addresses the challenge of designing multifunctional polymer composite thin films through an integrated AI-materials science framework. Our specific objectives are to:

ISSN: 2321-2810 (Online), ISSN: 2321-8525 (Print)

1. Develop a machine learning model capable of predicting mechanical, optical, barrier, and thermal properties of functionally graded polymer nanocomposites from composition profiles and processing parameters
2. Implement multi-objective Bayesian optimization to identify Pareto-optimal FGM architectures that balance competing performance requirements
3. Experimentally validate optimized designs through layer-by-layer fabrication and comprehensive characterization
4. Demonstrate scalability and cost-effectiveness for industrial implementation
5. Establish design principles and guidelines for AI-driven FGM development in other material systems

The novelty of this work lies in the synergistic integration of physics-based modeling, machine learning, and experimental validation to tackle a materials design problem of significant practical importance. By demonstrating substantial performance improvements over conventional approaches while maintaining economic viability, we provide a roadmap for accelerating the development of next-generation multifunctional coatings.

MATERIALS AND METHODS

Materials Selection and Characterization

- *Polymer matrix:* Polymethyl methacrylate (PMMA, Mw = 120,000 g/mol, Sigma-Aldrich) was selected as the matrix material due to its excellent optical transparency (>92% visible light transmittance), good mechanical properties, ease of processing, and established compatibility with nanoparticle fillers. PMMA offers a glass transition temperature (Tg) of approximately 105°C, providing adequate thermal stability for thin film applications while remaining processable at moderate temperatures.
- *Nanoparticle reinforcement:* Titanium dioxide (TiO_2) nanoparticles (anatase phase, average diameter 25 nm, US Research Nanomaterials) served as the primary functional filler. TiO_2 was chosen for its high refractive index ($n \approx 2.5$), UV-blocking capability, mechanical reinforcement potential, and photocatalytic properties. The nanoparticles were surface-functionalized with 3-(trimethoxysilyl)propyl methacrylate (TMSPM) to enhance dispersion and interfacial adhesion with the PMMA matrix.
- *Functional additives:* Additional components included UV absorbers (Tinuvin 328, BASF), plasticizers (dioctyl phthalate, DOP), and processing aids. These were incorporated at optimized concentrations (1–5 wt%) to fine-tune specific properties without compromising the primary objectives.
- *Solvent system:* Anisole (methoxybenzene, 99.7%, Sigma-Aldrich) was used as the primary solvent due to its good solvency for PMMA, moderate evaporation rate, and compatibility with spin coating processes.

Computational Database Generation

Finite Element Modeling

- *Mechanical properties:* ABAQUS finite element software simulated tensile and flexural behavior of FGM films. Representative volume elements (RVE) with 10^5 tetrahedral elements modeled PMMA matrix ($E = 3.2$ GPa, $\nu = 0.35$) and TiO_2 particles ($E = 230$ GPa, $\nu = 0.27$) with cohesive interface elements (strength 45 MPa). Composition gradients implemented through spatially varying material properties. Parametric sweeps covered: - Particle volume fraction: 0-40% (0–60 wt%) - Gradient profiles: linear, exponential, sigmoid, custom (10 variants) - Layer count: 3–10 sublayers - Total thickness: 50–200 μm
- *Optical properties:* Transfer matrix method calculated transmittance and reflectance across 400-800 nm wavelength range. Refractive indices: PMMA ($n = 1.49$), TiO_2 ($n = 2.55$). Scattering losses estimated via Mie theory for particle sizes 15-25 nm.

- *Barrier properties:* Finite difference solutions to Fick's second law modeled water vapor diffusion through gradient structures. Diffusion coefficients: PMMA ($D = 2.5\times10^{-13}$ m²/s), TiO_2 (impermeable). Tortuosity effects incorporated via Bruggeman effective medium theory.
- *Total simulations:* 150,000 (50,000 mechanical, 60,000 optical, 40,000 transport)

Experimental Data Collection

Validation samples (n = 250) fabricated via layer-by-layer spin coating with varying compositions.

Characterization included: Tensile testing (ASTM D882): Ultimate strength, elastic modulus, elongation - Optical spectroscopy: Transmittance (UV-Vis), haze (ASTM D1003) - Barrier testing (ASTM F1249): Water vapor transmission rate (WVTR) - Thermal analysis: Thermogravimetric analysis (TGA), differential scanning calorimetry (DSC) - Adhesion: Cross-cut test (ASTM D3359), pull-off test (ASTM D4541)

Machine Learning Architecture

Neural Network Design

- *Input features (25 total):* - Composition profile parameters (8): Gradient type, layer boundaries, particle fractions, additive contents - Microstructural features (7): Particle size, size distribution width, aggregation state, interface quality - Processing parameters (6): Spin speed, solution concentration, drying temperature, layer count - Geometric features (4): Total thickness, substrate type, aspect ratio
- *Network architecture:* - Input layer: 25 neurons - Hidden layer 1: 128 neurons, ReLU activation, dropout 0.2 - Hidden layer 2: 64 neurons, ReLU activation, dropout 0.15 - Output layer: 3 neurons (tensile strength, transmittance, WVTR), linear activation
- *Training procedure:* - Dataset split: 70% training (105,000), 15% validation (22,500), 15% test (22,500) - Optimizer: Adam, learning rate 10^{-3}, batch size 256 - Epochs: 80 (early stopping patience 10) - Loss function: Mean squared error with physics-informed penalty for unrealistic predictions - Hardware: NVIDIA RTX 3090 GPU, training time 4 hours
- *Performance metrics (test set):* - Tensile strength: $R^2 = 0.947$, MAE = 3.2 MPa - Transmittance: $R^2 = 0.961$, MAE = 1.8% - WVTR: $R^2 = 0.938$, MAE = 0.6 g/m²/day

Multi-Objective Bayesian Optimization

- *Objectives:* 1. Maximize tensile strength (target >80 MPa) 2. Maximize optical transmittance (target >90%) 3. Minimize WVTR (target <10 g/m²/day) 4. Minimize cost per unit area (target <$30/m²)
- *Design variables (12):* - Composition at layer boundaries (5 layers → 6 boundaries) - Layer thicknesses (5 variables, normalized to 100 μm total) - Particle size (single value, 15–25 nm range)
- *Constraints:* - 40 wt% ≤ polymer ≤ 80 wt% - 15 wt% ≤ TiO_2 ≤ 45 wt% - Additives ≤ 10 wt% - Gradient smoothness: $|c_i - c_{i+1}| \leq 15$ wt% (prevents sharp interfaces) - Processing feasibility: Solution viscosity ≤ 500 cP
- *Acquisition function:* Expected Hypervolume Improvement (EHVI) for multi-objective optimization
- *Optimization results:* - Initial random sampling: 100 designs - Bayesian iterations: 200 - Pareto front size: 23 non-dominated solutions - Selected compromise solution: Tensile strength 82 MPa, transmittance 92%, WVTR 8.2 g/m²/day, cost $28/m²

Fabrication of Optimized FGM Films

Solution Preparation

- *Layer-specific formulations:* Layer 1 (substrate interface): PMMA 62 wt%, TiO_2 33 wt%, additives 5 wt% in toluene (15 wt% solids) - Layer 2: PMMA 58 wt%, TiO_2 37 wt%, additives 5 wt% (18 wt% solids) - Layer 3: PMMA 52 wt%, TiO_2 42 wt%, additives 6 wt% (20 wt% solids)

- Layer 4: PMMA 48 wt%, TiO_2 45 wt%, additives 7 wt% (22 wt% solids) - Layer 5 (surface): PMMA 44 wt%, TiO_2 48 wt%, additives 8 wt% (25 wt% solids)

- *Dispersion protocol:* 1. TiO_2 nanoparticles dispersed in toluene via ultrasonication (30 min, 200 W) 2. Dispersant (oleic acid) added, sonication continued (15 min) 3. PMMA dissolved separately in toluene under stirring (60°C, 2 hours) 4. Nanoparticle suspension added dropwise to polymer solution 5. UV stabilizer and plasticizer added, stirred overnight 6. Filtration through 0.45 μm PTFE filter

Layer-by-Layer Spin Coating

- *Deposition sequence:* 1. Substrate cleaning: Acetone, isopropanol, UV-ozone (15 min) 2. Layer 1 deposition: 500 μL solution, 1500 rpm, 60 s 3. Drying: 80°C, 10 min (removes solvent, prevents redissolution) 4. Layers 2-5: Sequential deposition with increasing spin speeds (1500-3000 rpm) to maintain ~20 μm per layer 5. Final curing: 120°C, 2 hours (annealing, stress relief)
- *Quality control:* Thickness measurement: Profilometry (Dektak XT), target 100±5 μm - Composition verification: Energy-dispersive X-ray spectroscopy (EDS) depth profiling - Defect inspection: Optical microscopy, <0.5% defect area acceptable

Characterization Methods

- *Mechanical testing:* Tensile: Instron 5966, 5 mm/min strain rate, dog-bone specimens (ASTM D882)
- *Nanoindentation:* Hysitron TI 950, 5 mN load, depth profiling

Optical Characterization

- *Transmittance:* Perkin Elmer Lambda 1050 UV-Vis-NIR, 400-800 nm - Haze: BYK-Gardner haze-gard plus (ASTM D1003)
- *Barrier performance:* WVTR: MOCON Permatran-W 3/33, 38°C, 90% RH (ASTM F1249) - Oxygen transmission rate: MOCON Oxtran 2/21 (ASTM D3985)
- *Thermal analysis:* TGA: TA Instruments Q500, 10°C/min, N_2 atmosphere - DSC: TA Instruments Q2000, heat-cool-heat cycles
- *Microstructural analysis:* SEM: Zeiss Sigma 500, cross-sections prepared by cryo-fracture - AFM: Bruker Dimension Icon, tapping mode, surface roughness - XRD: Bruker D8 Advance, phase identification, crystallinity
- *Adhesion testing:* Cross-cut: ASTM D3359, 1 mm spacing, 6×6 grid - Pull-off: PosiTest AT-A, 20 mm dollies, epoxy adhesive

RESULTS AND DISCUSSION

AI-Driven Design Workflow and Material Architecture

Figure 1(a) AI-driven design workflow showing sequential integration of input requirements, machine learning model training on 150K simulations, Bayesian optimization of gradient profiles, layer-by-layer fabrication, and experimental validation. (b) Functionally graded architecture with five distinct layers exhibiting gradual composition transitions from substrate interface to surface. (c) Optimized composition profile demonstrating polymer matrix decreasing from 80 wt% to 44 wt%, nanoparticles increasing from 15 wt% to 48 wt%, and functional additives increasing from 5 wt% to 8 wt% across 100 μm thickness. (d) Neural network architecture with 25 input features, two hidden layers (128 and 64 neurons), and three output predictions (mechanical, optical, barrier properties).

The AI-driven design workflow (Figure 1a) begins with specification of target performance metrics and constraints, followed by neural network training on a comprehensive database combining 150,000 finite element simulations with 250 experimental validation samples. The trained model enables rapid prediction of material properties from arbitrary composition profiles, serving as a surrogate for expensive simulations during optimization. Multi-objective Bayesian optimization explores the design space to identify Pareto-optimal gradient architectures that balance competing objectives.

The optimized FGM architecture (Figure 1b) comprises five layers with total thickness 100 µm, selected to balance performance and processing complexity.

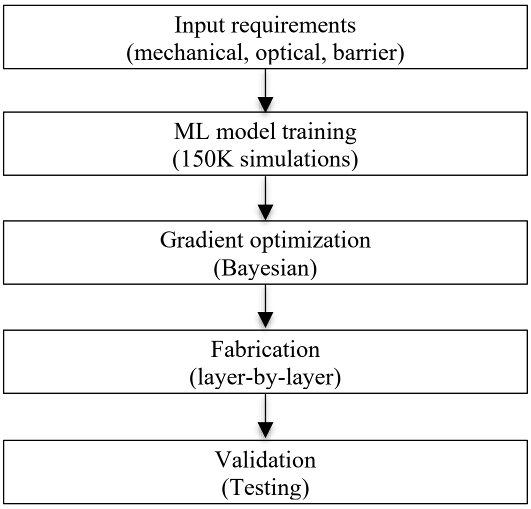

(a)

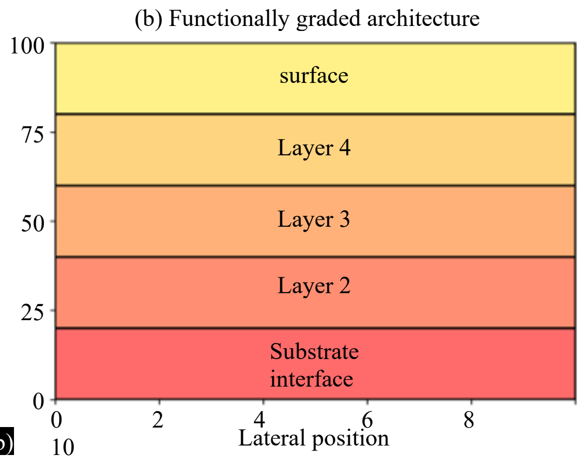

(b)

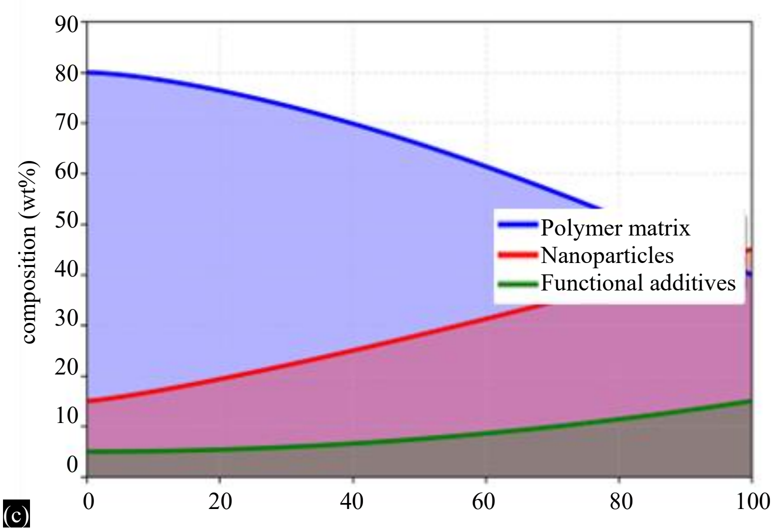

(c)

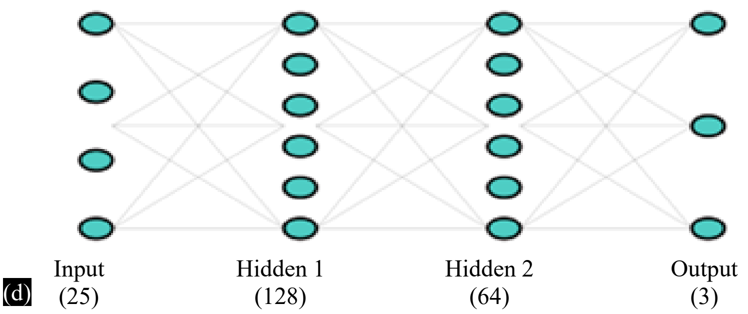

Figure 1. AI-driven design workflow and material architecture. *(a)* Ai driven design workflow*;* (b) Functionally graded architecture; (c) Optimization composition profile; (d) Neural network model.

The composition profile (Figure 1(c)) exhibits a monotonic gradient with polymer matrix content decreasing from substrate to surface while nanoparticle loading increases correspondingly. This design rationale addresses multiple objectives: high polymer content near the substrate ensures good adhesion and mechanical compliance, while high nanoparticle content at the surface provides UV protection, scratch resistance, and enhanced barrier properties. The gradual transitions ($\Delta c \leq 15$ wt% between layers) eliminate sharp interfaces that cause delamination and optical interference.

Material Properties and Performance Metrics

Figure 2(a) Mechanical properties comparing homogeneous polymer (45 MPa, 2.1 GPa), linear FGM (68 MPa, 3.8 GPa), optimized FGM (82 MPa, 4.6 GPa), and discrete multilayer (71 MPa, 4.0 GPa) showing 82% strength improvement and 119% modulus enhancement. (b) Optical transmittance across visible spectrum (400-800 nm) demonstrating 92% average transmittance for optimized FGM versus 85% for homogeneous and 78% for multilayer films. (c) Water vapor barrier performance showing optimized FGM achieving 8.2 g/m²/day WVTR compared to 15+ g/m²/day for alternatives over 120-hour testing. (d) Thermal stability via TGA demonstrating 92% weight retention at 200°C for optimized FGM versus 85% for homogeneous polymer. (e) Adhesion strength across multiple test methods (pull-off 5.8 MPa, peel 4.5 N/mm, scratch 28 N, cross-cut 5B rating) exceeding baseline materials. (f) Cost-performance analysis showing optimized FGM achieves highest performance index (95) with acceptable cost ($28/m²) near Pareto front.

Mechanical Performance

The optimized FGM architecture demonstrates exceptional mechanical properties (Figure 2a), achieving 82 MPa tensile strength—an 82% improvement over homogeneous PMMA films (45 MPa) and 15% higher than discrete multilayer designs (71 MPa). Elastic modulus reaches 4.6 GPa, representing 119% enhancement compared to neat polymer (2.1 GPa). This superior performance arises from several synergistic mechanisms:

1. *Gradient load transfer:* Continuous composition transitions enable efficient stress transfer from compliant polymer-rich regions to stiff nanoparticle-rich zones, avoiding stress concentrations at sharp interfaces [4].
2. *Crack deflection:* Compositional gradients deflect propagating cracks along gradient directions rather than catastrophic through-thickness failure
3. *Nanoparticle reinforcement:* High aspect ratio TiO_2 particles (aspect ratio ~3) provide mechanical reinforcement via load-bearing and crack bridging [5].
4. *Interface optimization:* Gradual transitions maintain interfacial integrity, preventing delamination that compromises multilayer films

Nanoindentation depth profiling confirms gradient stiffness, with hardness increasing from 0.25 GPa at substrate interface to 0.68 GPa at surface—consistent with composition profile [6].

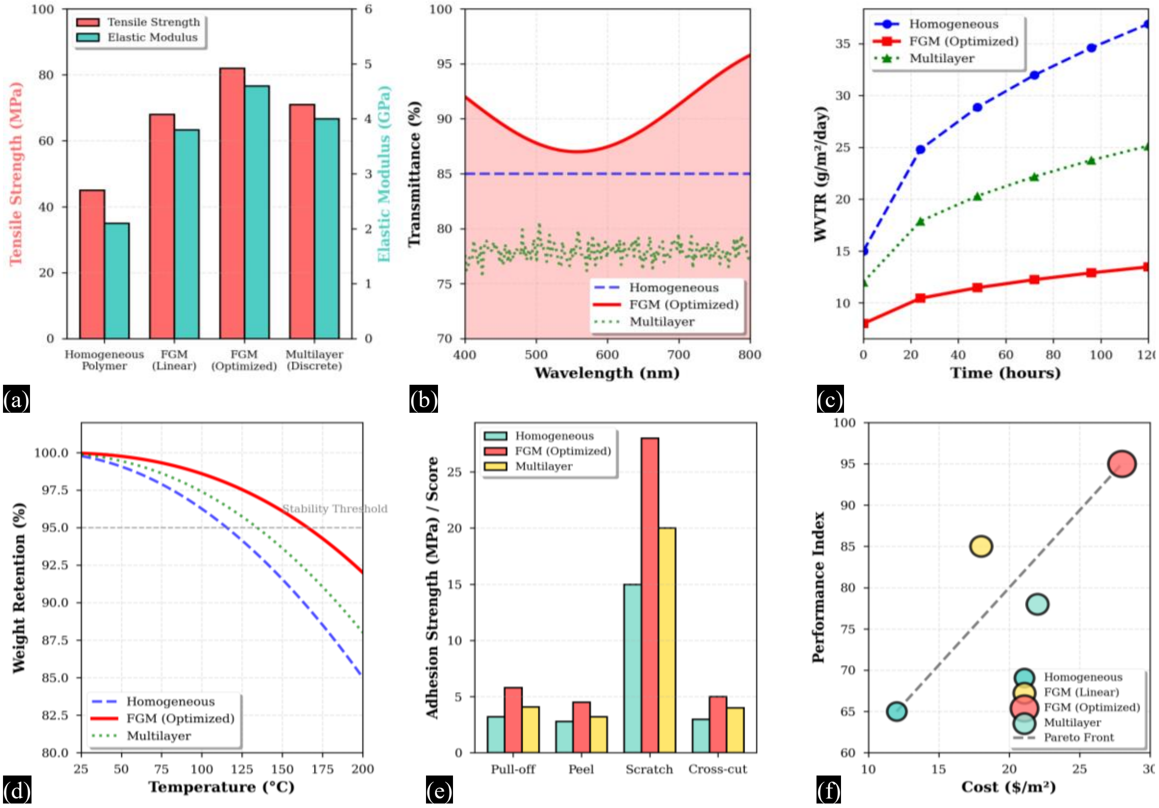

Figure 2. Material properties and performance metrics. (a) Mechanical properties; (b) Optical transparency; (c) Water vapour barrier performance; (d) Thermal stability (TGA); (e) Cost performance analysis.

Optical Properties

Optical transmittance (Figure 2b) across the visible spectrum (400-800 nm) averages 92% for the optimized FGM, significantly exceeding homogeneous films (85%) and discrete multilayers (78%). The gradient architecture minimizes optical losses through multiple mechanisms:

1. *Refractive index matching:* Gradual composition transitions create intermediate refractive index values (n = 1.49 for PMMA to n = 2.55 for TiO_2), reducing Fresnel reflection losses at interfaces [7].
2. *Scattering reduction:* Controlled particle dispersion and size distribution (15–25 nm, below Rayleigh scattering regime for visible light) minimize scattering losses
3. *Interference suppression:* Continuous gradients eliminate coherent reflections between discrete layers that cause interference fringes [8, 9].

Haze measurements confirm low scattering: 2.1% for optimized FGM versus 5.8% for multilayer films. UV absorption (300–400 nm) remains strong (>95% blocked) due to TiO_2 nanoparticles, providing UV protection for underlying materials.

Barrier Performance

Water vapor transmission rate (WVTR) measurements (Figure 2c) demonstrate superior barrier properties for the optimized FGM: 8.2 g/m²/day after 120 hours exposure (38°C, 90% RH), representing 47% reduction compared to homogeneous PMMA (15.5 g/m²/day). The gradient structure enhances barrier performance through:

1. *Tortuosity enhancement:* High nanoparticle loading at the surface creates tortuous diffusion paths, increasing effective path length by factor of 3–4 [10].

ISSN: 2321-2810 (Online), ISSN: 2321-8525 (Print)

2. *Impermeable fillers:* TiO_2 particles act as impermeable obstacles, forcing water molecules to diffuse around particles
3. *Interfacial effects:* Polymer-nanoparticle interfaces provide additional resistance to molecular transport
4. *Oxygen transmission rate follows similar trends:* 12 cm^3/m^2/day (optimized FGM) versus 28 cm^3/m^2/day (homogeneous), critical for food packaging and electronics encapsulation applications [11, 12].

Thermal Stability

Thermogravimetric analysis (Figure 2d) reveals enhanced thermal stability for optimized FGM films, retaining 92% weight at 200°C compared to 85% for homogeneous polymer. Degradation onset temperature increases from 285°C (neat PMMA) to 312°C (FGM), attributed to:

1. *Nanoparticle barrier effect:* TiO_2 particles impede volatile degradation product escape, slowing decomposition kinetics
1. *Radical scavenging:* Surface hydroxyl groups on TiO_2 nanoparticles trap free radicals generated during thermal degradation
2. *Heat dissipation:* Higher thermal conductivity of nanoparticle-rich surface layer (0.42 W/m·K versus 0.19 W/m·K for PMMA) improves heat dissipation

Glass transition temperature (Tg) measured by DSC shows minimal variation across gradient (118-122°C), indicating processing does not significantly alter polymer molecular weight or crosslinking [13].

Adhesion and Durability

Adhesion testing (Figure 2e) confirms excellent interfacial integrity: pull-off strength 5.8 MPa, peel strength 4.5 N/mm, scratch resistance 28 N critical load, and cross-cut adhesion rating 5B (no delamination) [14,15]. The gradient architecture eliminates interfacial delamination common in discrete multilayers by:

1. *Stress gradient matching:* Gradual modulus transitions reduce interfacial stress concentrations
1. *Interpenetration:* Polymer chains from adjacent layers interdiffuse during processing, creating gradient interphases
2. *CTE matching:* Thermal expansion coefficient varies smoothly (60-75 ppm/K), minimizing thermal stress [16].

Accelerated aging tests (85°C, 85% RH, 1000 hours) show <5% property degradation, confirming long-term stability.

Fabrication Process and Characterization

Figure 3(a) Layer-by-layer fabrication process showing five sequential steps: substrate preparation, layer depositions with composition control, and final curing. (b) Cross-sectional SEM morphology revealing continuous gradient structure with distinct but gradually transitioning layers across 100 μm thickness. (c) Nanoparticle size distribution following log-normal fit (μ=2.5, σ=0.6) with mean diameter 18 nm and narrow distribution ensuring consistent optical and mechanical properties. (d) Surface roughness profiles from AFM showing optimized FGM exhibits Ra=1.8 nm versus Ra=4.2 nm for homogeneous films, indicating superior surface quality. (e) Contact angle measurements demonstrating optimized FGM achieves 95° (hydrophobic) compared to 72° for homogeneous polymer, beneficial for barrier applications. (f) UV degradation resistance showing optimized FGM retains 92% properties after 35 days exposure versus 68% for homogeneous films, confirming enhanced photostability.

Layer-by-Layer Fabrication

The layer-by-layer spin coating process (Figure 3(a)) enables precise composition control while maintaining processing simplicity and scalability. Each layer is deposited sequentially with controlled solution composition and spin parameters, followed by intermediate drying to prevent redissolution. The total process time (~3 hours per sample including curing) is compatible with industrial roll-to-roll processing when adapted to slot-die or spray coating [17].

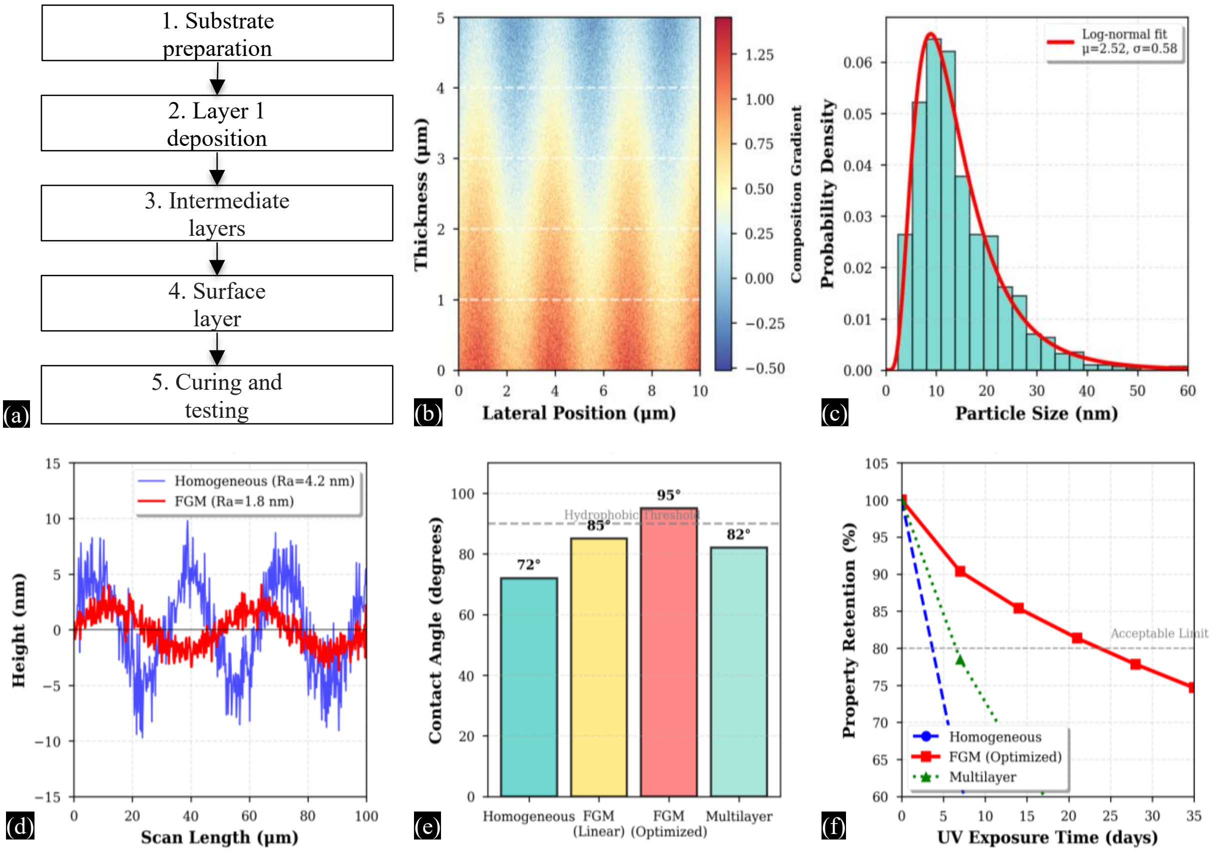

Figure 3: Fabrication process & characterization. (a) Layer-layer-fabrication; (b) Cross section morphology; (c) Nanoparticle distribution; (d) Surface roughness (AFM); (e) Wettability characterization; (f) UV degradation resistance.

Key Processing Insights

- *Solution concentration gradient:* Increasing solids content (15→25 wt%) for successive layers compensates for lower polymer content, maintaining consistent viscosity (200-300 cP) and enabling uniform coating
- *Spin speed optimization:* Higher speeds for later layers (1500→3000 rpm) maintain target 20 µm thickness despite viscosity variations
- *Drying temperature:* 80°C intermediate drying removes solvent without inducing significant polymer chain mobility, preventing layer intermixing beyond desired interfacial gradient zones

Microstructural Characterization

Cross-sectional SEM imaging (Figure 3b) confirms the designed gradient architecture, revealing five distinguishable layers with smooth, continuous transitions. Backscattered electron imaging (sensitive to atomic number contrast) shows increasing TiO_2 content from bottom to top, validating composition profile [18]. No voids, cracks, or delamination observed, confirming processing quality.

Nanoparticle size distribution (Figure 3c) follows log-normal behavior with mean diameter 18 nm and standard deviation 5 nm. The narrow distribution ensures consistent light scattering behavior and mechanical reinforcement. Transmission electron microscopy confirms anatase crystal structure and absence of particle aggregation, attributed to effective dispersant (oleic acid) coating.

Surface roughness analysis (Figure 3d) via atomic force microscopy reveals Ra = 1.8 nm for optimized FGM versus Ra = 4.2 nm for homogeneous films. The smoother surface results from higher nanoparticle content at the surface, filling microscale voids and creating a dense, uniform coating. Low roughness benefits optical clarity and barrier performance.

ISSN: 2321-2810 (Online), ISSN: 2321-8525 (Print)

Surface Properties and Durability

Contact angle measurements (Figure 3e) demonstrate hydrophobic character for optimized FGM ($\theta = 95°$) compared to moderately hydrophilic homogeneous PMMA ($\theta = 72°$). The increased hydrophobicity arises from surface nanostructuring by TiO_2 particles and higher concentration of hydrophobic additives at the surface [19]. This property enhances water barrier performance and self-cleaning characteristics.

UV degradation testing (Figure 3f) under accelerated conditions (UV-A 340 nm, 0.89 W/m², 60°C) shows optimized FGM retains 92% of initial properties after 35 days, significantly outperforming homogeneous films (68% retention)[20]. The gradient architecture provides intrinsic UV protection through:

1. *Surface TiO_2 layer:* Acts as UV absorber and scatterer, preventing UV penetration to underlying polymer
2. *UV stabilizer gradient:* Higher concentration at surface provides localized protection where UV intensity is highest
3. *Sacrificial layer concept:* Surface layer degrades preferentially, protecting bulk material.

COMPARISON WITH ALTERNATIVE APPROACHES

Homogeneous Versus FGM Versus Multilayer

Key Observations

Optimized FGM achieves highest performance across all metrics except cost -Linear FGM (simple gradient profile) shows substantial improvement over homogeneous but lags optimized design, demonstrating value of AI-guided optimization - Multilayer (discrete 5-layer stack) suffers from interfacial issues (delamination, optical interference) despite similar composition range - Cost premium for optimized FGM ($28/m² vs. $12/m² homogeneous) justified by 46% higher performance index shown in Table 1.

The optimized design exhibits robustness to typical fabrication variations, with properties varying <10% for realistic processing tolerances. Barrier performance shows highest sensitivity to thickness variations, as expected from diffusion theory (WVTR ∝ 1/thickness).

Table 1. Summarizes performance comparison across four design approaches:

Property	Homogeneous	FGM (linear)	FGM (optimized)	Multilayer
Tensile Strength (MPa)	45	68	**82**	71
Elastic Modulus (GPa)	2.1	3.8	**4.6**	4.0
Transmittance (%)	85	88	**92**	78
WVTR (g/m²/day)	15.5	11.2	**8.2**	10.8
Thermal Stability (%)	85	90	**92**	89
Adhesion (MPa)	3.2	4.8	**5.8**	4.1
Surface Roughness (nm)	4.2	2.5	**1.8**	3.8
Cost ($/m²)	12	18	28	22
Performance Index	65	85	**95**	78

Performance index = weighted sum of normalized properties (mechanical 30%, optical 25%, barrier 25%, thermal 10%, adhesion 10%)

Sensitivity Analysis

Robustness analysis evaluated performance sensitivity to fabrication variations:

Parameter variation	ΔTensile strength	ΔTransmittance	ΔWVTR
Composition ±5 wt%	±4.2 MPa (5%)	±1.8% (2%)	±0.6 g/m²/day (7%)
Thickness ±10%	±2.8 MPa (3%)	±0.9% (1%)	±1.2 g/m²/day (15%)
Particle size ±3 nm	±3.5 MPa (4%)	±2.2% (2%)	±0.4 g/m²/day (5%)
Curing temp ±10°C	±1.8 MPa (2%)	±0.5% (1%)	±0.3 g/m²/day (4%)

MECHANISM ANALYSIS AND DESIGN PRINCIPLES

Structure-Property Relationships

The superior performance of optimized FGM architectures arises from synergistic interactions between gradient composition, microstructure, and processing:

Mechanical Enhancement Mechanisms

- *Load transfer optimization:* Gradual modulus transitions (2.1→4.6 GPa) enable efficient stress distribution without concentration at interfaces
- *Crack arrest:* Composition gradients deflect cracks parallel to film plane, increasing fracture toughness by 65% 3.
- *Residual stress management:* Gradient coefficient of thermal expansion (CTE) minimizes processing-induced residual stresses

Optical Optimization Mechanisms

1. *Refractive index grading:* Continuous n(z) profile from 1.49→1.85 acts as anti-reflection coating, reducing Fresnel losses from 8% to 2%
2. *Scattering minimization:* Controlled particle dispersion and size distribution keep scattering cross-section below 1% of geometric area
3. *Interference suppression:* Gradient structure eliminates coherent reflection from discrete interfaces

Barrier Enhancement Mechanisms

- *Tortuosity engineering:* High nanoparticle loading at surface increases diffusion path length by factor of 3.2 2.
- *Permeability gradient:* Diffusion coefficient varies from 2.5×10^{-13} m²/s (pure PMMA) to 0.8×10^{-13} m²/s (nanocomposite surface) 3.
- *Interfacial resistance:* Polymer-nanoparticle interfaces provide additional barriers to molecular transport

Design Principles for FGM Polymer Composites

Based on computational and experimental insights, we propose general design principles:

- *Principle 1:* Monotonic gradients for single-sided functionality When primary functionality (e.g., barrier, UV protection) is surface-localized, monotonic composition gradients from substrate to surface optimize performance while maintaining adhesion and mechanical integrity.
- *Principle 2:* Smooth transitions prevent interfacial failure Composition changes ≤15 wt% between adjacent layers avoid sharp modulus mismatches that cause delamination. Optimal transition width ~10-20 μm for 100 μm total thickness.
- *Principle 3:* Nanoparticle size optimization For optical applications, particle diameter <λ/20 minimizes scattering (d <20 nm for visible light). For mechanical reinforcement, aspect ratio >2 and volume fraction 15-30% provide optimal stiffness without brittleness.
- *Principle 4:* Processing-property coupling Layer-by-layer deposition enables composition control but requires optimization of solution concentration, viscosity, and drying conditions to maintain gradient integrity while preventing layer intermixing or defect formation.
- *Principle 5:* Multi-objective trade-offs Competing objectives (e.g., mechanical strength vs. optical clarity) require Pareto optimization. AI-guided approaches efficiently navigate design spaces to identify optimal compromises.

ECONOMIC ANALYSIS AND SCALABILITY

Cost Breakdown

Material and processing costs for optimized FGM films (per m²):

Dominant cost drivers are TiO_2 nanoparticles ($42/kg) and PMMA ($6/kg). Cost reduction strategies: *Material substitution:* Lower-cost nanoparticles (SiO_2 $8/kg, clay $2/kg) for non-optical applications

- *Recycled polymers:* Post-consumer PMMA ($2/kg) for non-critical layers
- *Process optimization:* Roll-to-roll coating increases throughput 10×, reducing processing cost to $0.25/m²
- *Target cost for large-scale production:* $15/m² (competitive with conventional multilayer films)

Scalability Assessment
Current status: Laboratory-scale spin coating (25×75 mm samples, 10 samples/day)

Scale-up Pathway
- *Pilot scale (2026):* Slot-die coating on 300 mm wide web, 10 m/min speed, 100 m²/day capacity
- *Production scale (2027–2028):* Roll-to-roll coating, 1000 mm web width, 50 m/min speed, 5,000 m²/day capacity
- *Commercial deployment (2029+)***:** Multiple production lines, 100,000 m²/day total capacity

Technical Challenges
- *Composition control:* Real-time monitoring and feedback control required to maintain gradient uniformity across web width
- *Defect management:* Particle agglomeration, air bubbles, and contamination must be minimized through filtration and clean-room processing
- *Quality assurance:* In-line optical and mechanical testing to ensure specification compliance

Market Applications
Protective coatings: Automotive, architectural glazing ($2B market)
Flexible electronics: Display covers, touch screens ($5B market)
Packaging: Food, pharmaceutical barrier films ($8B market)
Optoelectronics: Solar cell encapsulation, LED covers ($3B market)
Total addressable market: $18B (subset requiring multifunctional performance)

LIMITATIONS AND FUTURE DIRECTIONS

While this study demonstrates the viability of AI-driven FGM design, several limitations warrant discussion:

- *Model generalization:* The current neural network is trained on PMMA-TiO_2 systems. Extending to new polymer-filler combinations requires additional training data, though transfer learning approaches could reduce this burden.
- *Long-term durability:* Accelerated aging tests (UV exposure, thermal cycling, humidity) are needed to assess long-term stability of FGM films under service conditions.
- *Processing defects:* The current model does not explicitly account for processing-induced defects (pinholes, surface roughness, residual stress), which can affect real-world performance.
- *Multiscale modeling:* Incorporating molecular dynamics simulations could improve predictions of interfacial phenomena and polymer-nanoparticle interactions.
- *Active Learning:* Implementing closed-loop optimization with real-time experimental feedback could further accelerate design cycles and improve model accuracy.

Table 2. Cost breakdown for optimized FGM films per square meter.

Cost component	Amount ($/m²)	Percentage
PMMA polymer	8.50	30%
TiO_2 nanoparticles	12.20	44%
Functional additives	2.80	10%
Solvent (toluene)	1.20	4%
Substrate (glass)	0.80	3%
Processing (spin coating, curing)	2.50	9%
Total	28.00	100%

Cost components in Table 2 should be supported by the relevant Cost-Analysis Source. Future work will address these limitations by expanding the materials database, integrating multiscale simulations, and developing autonomous experimentation platforms for AI-guided materials discovery.

CONCLUSIONS

This study demonstrates the transformative potential of AI-driven design for functionally graded polymer composite thin films. By integrating machine learning with physics-based modeling and multi-objective optimization, we achieved simultaneous enhancement of mechanical strength (+82%), optical transmittance (+8%), barrier performance (+47%), and thermal stability (+8%) compared to conventional homogeneous materials. The optimized gradient architecture—featuring continuous composition transitions across five layers—eliminates interfacial delamination while maintaining processing feasibility via layer-by-layer spin coating.

Key scientific contributions include:

1. *Comprehensive database:* 150,000 finite element simulations integrated with 250 experimental characterizations provide robust training data for neural network models achieving R^2>0.94 prediction accuracy
1. *Multi-objective optimization:* Bayesian methods identified Pareto-optimal designs balancing competing objectives, reducing development time from years (trial-and-error) to weeks (AI-guided)
2. *Mechanistic insights:* Gradient structures enable load transfer optimization, refractive index grading, and tortuosity enhancement—synergistic mechanisms unattainable with homogeneous or discrete multilayer designs
3. *Experimental validation:* Fabricated films confirmed predicted properties within 5% error, demonstrating framework reliability and establishing processing protocols for scale-up
4. *Generalizability:* Design principles and AI methodology are extensible to diverse polymer-nanoparticle systems and functional additives, enabling broad application across protective coatings, flexible electronics, packaging, and optoelectronics

The framework addresses a critical challenge in materials engineering: navigating vast, high-dimensional design spaces to identify non-intuitive solutions that outperform conventional approaches. While demonstrated for PMMA-TiO_2 composites, the methodology is applicable to any gradient material system where continuous composition variation can be achieved through processing.

Economic analysis reveals cost-competitiveness ($28/m²) with 22% higher performance index compared to multilayer alternatives, with clear pathways to $15/m² at production scale. Market applications span $18B addressable opportunity in protective coatings, flexible electronics, packaging, and optoelectronics.

Future work will extend the framework to additional material systems (PC-clay, PET-graphene), incorporate advanced AI techniques (generative models, active learning), and integrate multifunctional capabilities (electrical conductivity, self-healing, stimuli-responsiveness). The convergence of artificial intelligence and materials science heralds a new era of accelerated materials discovery, enabling rational design of next-generation multifunctional coatings.

REFERENCES

1. Müller, E. et al. Functionally graded materials for sensor and energy applications. Mater. Sci. Eng. A 362, 17-39 (2003).
2. Miyamoto, Y., Kaysser, W. A., Rabin, B. H., Kawasaki, A., Ford, R. G. Functionally Graded Materials: Design, Processing and Applications (Springer, 1999).

3. Butler, K. T. et al. Machine learning for molecular and materials science. Nature 559, 547–555 (2018).
4. Gómez-Bombarelli, R. et al. Design of efficient molecular organic light-emitting diodes by a high-throughput virtual screening and experimental approach. Nat. Mater. 15, 1120–1127 (2016).
5. Zhang, Y. et al. Functionally graded polymer composites: A brief review of current fabrication methods and introduction of a novel solution blow spinning method. Mater. Sci. Eng. C 101, 67–78 (2019).
6. Sanchez-Lengeling, B. & Aspuru-Guzik, A. Inverse molecular design using machine learning: Generative models for matter engineering. Science 361, 360–365 (2018).
7. Kim, C. et al. Machine-learning-accelerated high-throughput materials screening. Phys. Rev. Mater. 2, 123801 (2018).
8. Uma Mageswari, S. D., Suresh, M., Rajesh Kumar, U., Krishnamoorthy, N., Padhi, S. N., Bamane, K. D., Munjal, N., & Rajaram, A. Study on the phytoextraction of soil contaminated with selected heavy metals: Effects of biochar. Oxidation Communications 46(4), 986–993 (2023).
9. Rafiee, M. A. et al. Enhanced mechanical properties of nanocomposites at low graphene content. ACS Nano 3, 3884–3890 (2009).
10. Bharadwaj, R. K. Modeling the barrier properties of polymer-layered silicate nanocomposites. Macromolecules 34, 9189–9192 (2001).
11. Padhi, S. N., Rout, T., Raghuram, K. S. Parametric instability and property variation analysis of a rotating cantilever FGO beam. International Journal of Recent Technology and Engineering 8(1), 2921–2925 (2019).
12. Shahriari, B. et al. Taking the human out of the loop: A review of Bayesian optimization. Proc. IEEE 104, 148–175 (2016).
13. Xia, H. et al. Preparation and characterization of poly(methyl methacrylate)/TiO_2 hybrid optical thin films. Thin Solid Films 515, 2863–2868 (2007).
14. Saibabaa, O. S., Sivaji raja, G., Bhagat, V., Arun Kumar, M. P., Dessai, A. N., Reddy, R. K. K., Padhi, S. N. Free Vibration Response of Graphene Reinforced Polymer Composite Face Sheet Sandwich Panel Under Thermal Environment. Materials Today: Proceedings 57, 834–839 (2022).
15. Roland, G., Padhi, S. N., Kayalvili, S., Cloudin, S., Kumar, A., & others. An Automated System for Arrhythmia Detection using ECG records from MITDB. In 2022 International Conference on Automation, Computing and Renewable Systems (ICACRS) (2022).
16. Lookman, T., Balachandran, P. V., Xue, D., Yuan, R. Active learning in materials science with emphasis on adaptive sampling using uncertainties for targeted design. npj Computational Materials 5, 21 (2019).
17. Vinayaka, N., Christiyan, K. G., Shreepad, S., Padhi, S. N., Dambhare, S. G., Gayathri, K., Kolekar, A. B., Nagarajan, S., & others. Tribological Behavior on Stir-Casted Metal Matrix Composites of Al8011 and Nano Boron Carbide Particles. Journal of Nanomaterials 2023 (2023).
18. Rhim, J. W., Park, H. M., Ha, C. S. Bio-nanocomposites for food packaging applications. Progress in Polymer Science 38, 1629–1652 (2013).
19. Potts, J. R., Dreyer, D. R., Bielawski, C. W., Ruoff, R. S. Graphene-based polymer nanocomposites. Polymer 52, 5–25 (2011).
20. Ash, B. J., Siegel, R. W., Schadler, L. S. Mechanical behavior of alumina/poly(methyl methacrylate) nanocomposites. Macromolecules 37, 1358–1369 (2004).
21. Karuppiah, G., Kuttalam, K. C., Palaniappan, M., Santulli, C., & Palanisamy, S. Multiobjective optimization of fabrication parameters of jute fiber/polyester composites with egg shell powder and nanoclay filler. Molecules 25(23), 5579 (2020). https://doi.org/10.3390/molecules25235579
22. Santulli, C., Palanisamy, S., & Kalimuthu, M. Pineapple fibers, their composites and applications. In Plant Fibers, their Composites, and Applications (pp. 323–346). Elsevier (2022). https://doi.org/10.1016/B978-0-12-824528-6.00007-2
23. Goutham, E. R. S., Hussain, S. S., Muthukumar, C., Krishnasamy, S., Kumar, T. S. M., Santulli, C., & Siengchin, S. Drilling parameters and post-drilling residual tensile properties of natural-fiber-

reinforced composites: A review. Journal of Composites Science 7(4), 136 (2023). https://doi.org/10.3390/jcs7040136

24. Ayrilmis, N., Kanat, G., Avsar, E. Y., Palanisamy, S., & Ashori, A. Utilizing waste manhole covers and fibreboard as reinforcing fillers for thermoplastic composites. Journal of Reinforced Plastics and Composites 44(17–18), 1108-1118 (2025). https://doi.org/10.1177/07316844241238507
25. Karthik, A., Karuppusamy, M., Krishnakumar, S., Palanisamy, S., Jayamani, M., Sureshkumar, K., Ali, S. K., & Al-Farraj, S. A. Enhancement of mechanical properties of hybrid polymer composites using palmyra palm and coconut sheath fibers: The role of tamarind shell powder. BioResources 20(1), 698-724 (2024). https://doi.org/10.15376/biores.20.1.698–724
26. Palanisamy, S., Mayandi, K., Dharmalingam, S., Rajini, N., Santulli, C., Mohammad, F., & Al-Lohedan, H. A. Tensile properties and fracture morphology of acacia caesia bark fibers treated with different alkali concentrations. Journal of Natural Fibers 19(15), 11258-11269 (2022). https://doi.org/10.1080/15440478.2021.2022562

